Research Article Vol. 38, No. 9 / September 2021 / Journal of the Optical Society of America B 2455

Journal of the Optical Society of America B

OPTICAL PHYSICS

Ultrafast laser inscription of asymmetric integrated waveguide 3 dB couplers for astronomical K-band interferometry at the CHARA array

Aurélien Benoît,[1,*,†] Fraser A. Pike,[1,†] Tarun K. Sharma,[2,†] David G. MacLachlan,[1] Aline N. Dinkelaker,[3] Abani S. Nayak,[3] Kalaga Madhav,[3] Martin M. Roth,[3] Lucas Labadie,[2] Ettore Pedretti,[4] Theo A. ten Brummelaar,[5] Nic Scott,[6] Vincent Coudé du Foresto,[7] and Robert R. Thomson[1]

[1]SUPA, Institute of Photonics and Quantum Sciences, Heriot-Watt University, Edinburgh, EH14 4AS, UK
[2]I. Physikalisches Institut der Universität zu Köln, Zülpicher Strasse 77, 50937 Cologne, Germany
[3]Leibniz-Institut für Astrophysik Potsdam, An der Sternwarte 16, 14482 Potsdam, Germany
[4]UKRI STFC Rutherford Appleton Laboratory, Chilton, UK
[5]Center for High Angular Resolution Astronomy, Georgia State University, P.O. Box 3969, Atlanta, Georgia 30302-3969, USA
[6]NASA Ames Research Center, Moffett Field, California 94035, USA
[7]LESIA of Paris Observatory/CNRS/UPMC/Univ. Paris Diderot, Paris, France
*Corresponding author: a.benoit@hw.ac.uk

Received 1 March 2021; revised 11 June 2021; accepted 15 June 2021; posted 15 June 2021 (Doc. ID 423727); published 4 August 2021

We present the fabrication and characterization of 3 dB asymmetric directional couplers for the astronomical K-band at wavelengths between 2.0 and 2.4 μm. The couplers were fabricated in commercial Infrasil silica glass using an ultrafast laser operating at 1030 nm. After optimizing the fabrication parameters, the insertion losses of straight single-mode waveguides were measured to be ∼1.2 ± 0.5 dB across the full K-band. We investigate the development of asymmetric 3 dB directional couplers by varying the coupler interaction lengths and by varying the width of one of the waveguide cores to detune the propagation constants of the coupled modes. In this manner, we demonstrate that ultrafast laser inscription is capable of fabricating asymmetric 3 dB directional couplers for future applications in K-band stellar interferometry. Finally, we demonstrate that our couplers exhibit an interferometric fringe contrast of >90%. This technology paves the path for the development of a two-telescope K-band integrated optic beam combiner for interferometry to replace the existing beam combiner (MONA) in Jouvence of the Fiber Linked Unit for Recombination (JouFLU) at the Center for High Angular Resolution Astronomy (CHARA) telescope array.

https://doi.org/10.1364/JOSAB.423727

1. INTRODUCTION

The burgeoning field of astrophotonics has emerged over the past couple of decades and seeks to exploit photonic technologies and principles to enable the development of superior astronomical instruments [1–4]. Astrophotonics has already resulted in multiple successes, examples of which include the use of optical fibers for flexibly routing light from the telescope focal plane to spectrographs for analysis [5] and spectral imaging [6,7], and broadband laser frequency combs that provide unprecedented spectrograph calibration capabilities [8]. A raft of new and potentially transformative astrophotonic technologies is also currently under development. These include integrated echelle gratings [9], integrated fiber-fed spectrographs [10,11], waveguide Bragg gratings to filter out atmospheric OH lines [12–14], and ring-resonator-based frequency combs [15].

One of the most impressive successes in the astrophotonics field is the development of compact integrated optic (IO) beam combiners for coherently combining the light collected by multiple telescopes [16]. Beam combining instruments that utilize IO beam combiners, such as GRAVITY [17] or Precision Integrated-Optics Near-infrared Imaging ExpeRiment (PIONIER) [18] at the Very Large Telescope Interferometer (VLTI) telescope array [19], have demonstrated excellent capabilities. Despite these instruments, current IO

beam combiners require improvements to facilitate future scalability and additional applications. First, the number of telescopes might increase to enable more interferometric baselines. Secondly, to optimize IO beam combiners for specific applications, the design might have to be iteratively changed and improved, requiring flexibility in the manufacturing process. Once the design is fixed, however, production of identical devices is required, e.g., for space applications [20,21], where a large number of devices are needed for testing, qualification, and redundancy. Additionally, the IO devices used in GRAVITY and PIONIER are fabricated using conventional planar silica-on-silicon platforms that operate efficiently in the H-band (1.5–1.8 μm) but less so at longer wavelengths [22–24]. Applications in the K-band (2.0–2.4 μm), for example, are faced with unwanted propagation losses in silica-on-silicon platforms due to the OH contaminations in the glass [25]. Using existing IO beam combiner technology to go further into the mid-infrared (IR) therefore presents a challenge. Alternative methods, such as fluorine or chalcogenide fibers, are required to access this wavelength range, which enables us to access the fingerprint region with an abundance of fundamental absorption bands of chemical species from 3 to 20 μm and can improve imaging of extrasolar planets by reducing the contrast between starlight and planet compared to the visible range [26,27]. In this context, ultrafast laser inscription (ULI), with its capacity to inscribe an inexpensive 3D low-loss waveguide in a suitable glass, is an excellent candidate for expanding the working wavelength range of IO beam combiners. This fabrication technique has recently demonstrated a variety of different 3D complex-light reformatting components for operation in the H-, L-, and M-bands with experimental laboratory results as well as some "on-sky" measurements at near-IR wavelengths [28–31] and the Guided-Light Interferometric Nulling Technology (GLINT) instrument is a permanent module on the Subaru Coronagraphic Extreme Adaptive Optics (SCExAO) system at the Subaru telescope [32].

The Center for High Angular Resolution Astronomy (CHARA) [33] of Georgia State University uses a fiber-based beam combiner technology for two-telescope interferometry in the K-band: the Fiber Linked Unit for Recombination (FLUOR) utilizes fluoride fibers. In 2014, as part of the program known as Jouvence of FLUOR (JouFLU), major upgrades were applied including the fiber-fed interferometric beam combiner in a closed box system called MONA, achieving accurate interferometric visibility amplitude measurements with 0.1%–0.3% precision [34]. In the years since the upgrade, JouFLU has provided detailed measurements of the survey of debris-disc stars, and visibility estimation for the Exozodi survey [35,36]. Over time, however, it has started to experience technical challenges, including performance degradation, which makes high-resolution astronomy in the K-band difficult. An IO beam combiner could revive the JouFLU setup and K-band interferometry. With this in mind, we have started work to develop a two-input IO beam combiner that can become a replacement for the existing combiner, utilizing the infrastructure and optical setup of JouFLU at the CHARA array. A key enabler of this component is achromatic 3 dB couplers, the development of which we report here.

2. OVERVIEW OF A FUTURE IO BEAM COMBINER FOR JouFLU

Figure 1 presents a schematic illustration of the fiber-fed chip-based interferometric beam combiner we are developing for JouFLU, with an interface designed for the replacement of the existing MONA fiber beam combiner. Shown are the two input fibers that couple light into the ULI written waveguides on the glass substrate via a V-groove array. From the input waveguides, light is distributed to two photometric tap couplers (Tap) and two interferometric arms in the 3 dB directional coupler (3 dB) [37,38]. After the coupling region, the four outputs are connected to fibers arranged in a square array for coupling into the Near Infrared Camera and Multi-Object Spectrometer (NICMOS) camera.

Here, we investigate the potential of ULI fabrication to produce a 3 dB asymmetric IO beam combiner in Infrasil glass (IG) with the same MONA interferometric contrast around 90% for stellar interferometry over the full K-band. The paper is structured as follows. We present in Section 3 the manufacturing method and optimum parameters to obtain a low-loss 3 dB asymmetric coupler. In Section 4, we perform initial tests of the polarization behavior of the couplers and demonstrate the capacity of the integrated couplers to provide high contrast interferometry results. We present the conclusions of the paper in Section 5.

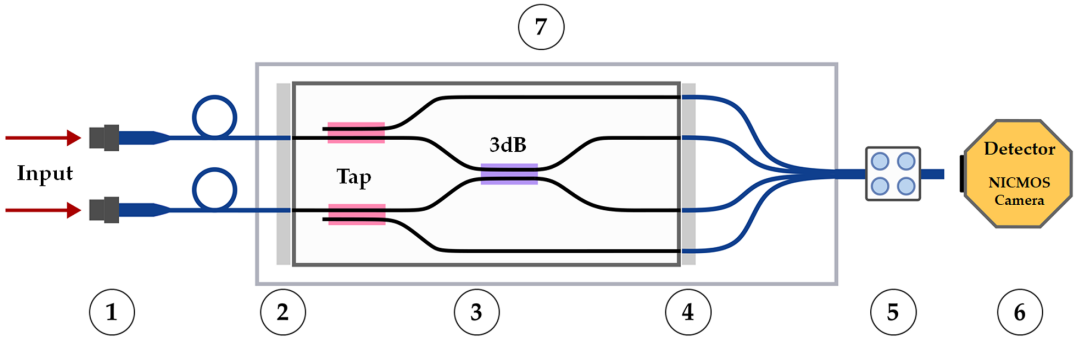

Fig. 1. Schematic representation of the IO beam combiner being developed for JouFLU with the fiber-coupled inputs from two telescopes connected to the chip via V-grooves, ULI written waveguides for the photometric tap as well as the 3 dB direct coupler, and output fiber bundle going to the NICMOS camera and detection system. (1) Light input from the telescope via FC/PC connectors, (2) input two-fiber V-groove array, (3) 3 dB asymmetric coupler and photometric tap couplers, (4) output four-fiber V-groove array, (5) fiber square bundle to (6) NICMOS detector, and (7) full packaged beam combiner system.

3. DEVELOPING K-BAND WAVEGUIDES

A. ULI Fabrication Details

To obtain low-loss guidance in the K-band, it is necessary to use a substrate material that exhibits low absorption in the 2.0–2.4 μm spectral range. To this end, we have chosen to focus our attention on using IG as a substrate for the ULI process. To perform the ULI process, we used a LightConversion Pharos laser at 1030 nm that delivers 185 fs pulses at a pulse repetition rate of 500 kHz, with the light polarization adjusted to circular. All structures were written using a transverse writing geometry and the multiscan technique to control the waveguide cross section [39]. Accordingly, the train of ultrafast laser pulses was focused ∼250 μm below the surface of the IG substrate using a 6.24 mm focal length lens with a numerical aperture (NA) of 0.4 (Thorlabs C110 TME-B), and waveguides were formed by translating the substrate through the laser focus in the plane perpendicular to the laser beam propagation axis.

B. Characterizing ULI Fabricated Waveguides

The insertion losses of the ULI waveguides were characterized using the system shown schematically in Fig. 2. The system consists of a supercontinuum (SC) source (NKT Extreme-K) followed by a bandpass filter (BPF) for 2250 ± 250 nm (Thorlabs FB2250-500) to select the K-band wavelength span. Figure 2 presents the two steps to characterize the insertion losses of the ULI waveguides. Light from the SC source is coupled into a 2 m long commercial fiber (NuFern SM1950).

To measure the insertion loss of the waveguide, a reference spectrum is first acquired using an IR fiber-coupled optical spectrum analyzer (Thorlabs OSA205). A few percent of the input light is used to monitor the stability of the input power during the measurements. In the second step, the NuFern fiber is cleaved close to its mid-point, and the cleaved ends are coupled to the ULI waveguide under test by butt-coupling with index matching fluid to reduce Fresnel reflections. Two three-axis translation stages were used to optimize the coupling of light between the ULI waveguide and the fibers. The spectra of the light coupled through the waveguide are acquired and compared to the reference spectrum to obtain the insertion loss across the K-band. After investigating a wide range of pulse energies for fabrication (from 33 to 255 nJ) and multiscan parameters (25 to 75 scans in steps of five and then 21 to 33 scans in steps of two), we found that optimal waveguides were fabricated using a pulse energy of 250 nJ (measured before the lens used to focus the light into the substrate), 31 scans of the substrate through the laser focus, with a scan separation of 200 nm, and a substrate translation velocity of $4\ \text{mm} \cdot \text{s}^{-1}$, corresponding to an estimated physical waveguide width of 6.2 μm. Figure 3(a) presents the insertion loss spectrum (black squares) where each point corresponds to a raw data average over a wavelength span of 8 nm, for a 17 mm long waveguide fabricated using the above-mentioned parameters. The throughput of these ULI waveguides is $\sim 1.2 \pm 0.5$ dB. We estimate that a minimum of approximately 0.02 dB/facet of this is due to coupling losses between the fiber and waveguide due to mode mismatch since the waveguide exhibits a mode field diameter (MFD) of ∼9.8 μm, and the fiber exhibits a MFD of ∼8.7 μm without any transverse offset. This leads us to conclude that the waveguides exhibit a maximum propagation loss of $\sim 0.68\ \text{dB} \cdot \text{cm}^{-1}$. This throughput value is of the same order of magnitude as previous single-mode ULI waveguide fabrications with $0.8\ \text{dB} \cdot \text{cm}^{-1}$ at 3.39 μm [40] or $0.85\ \text{dB} \cdot \text{cm}^{-1}$ at 1.3 μm [31].

The inset of Fig. 3(a) presents a micrograph of a ULI waveguide fabricated using the optimal ULI parameters where the incident writing laser beam comes from the top, and the writing process is from the left to right in Fig. 3(a). The insets of Fig. 3(b) show the recorded near-field intensity distributions recorded using a DataRay WinCamD microbolometer array for the fiber (F) and for the waveguide (W) with a magnification of around 67. From these near-field intensity distributions, the ULI waveguide MFD is measured around 10.3 μm on x axis and 9.3 μm on y axis at $1/e^2$ in comparison with the fiber MFD

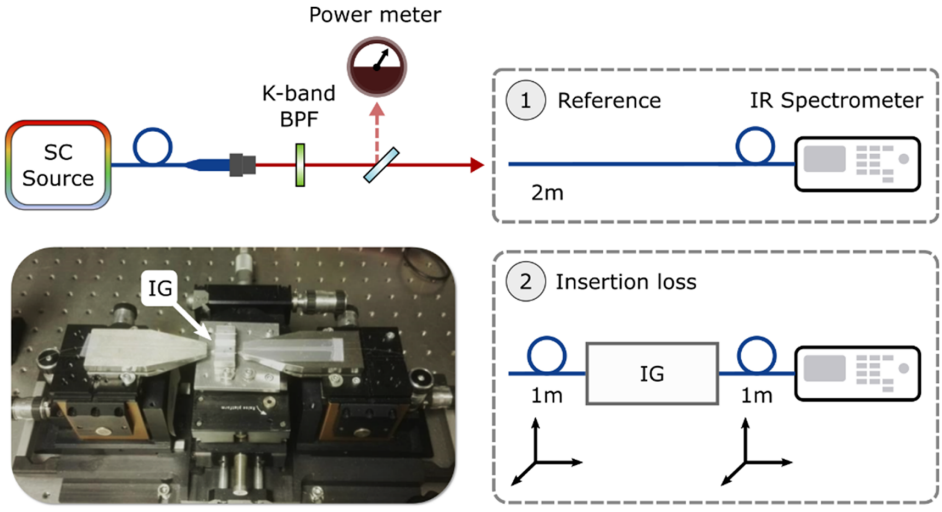

Fig. 2. Schematic representation of the experimental setup used for the waveguide and coupler characterization, based on a SC source followed by a K-band bandpass filter (BPF). Illustration of the two main steps of insertion loss measurements, with spectra measured directly for a 2 m fiber, followed by spectra for the cleaved fiber to measure insertion loss of the waveguide in IG. Inset: photograph of the double three-axis translation stage with the fibers and the IG.

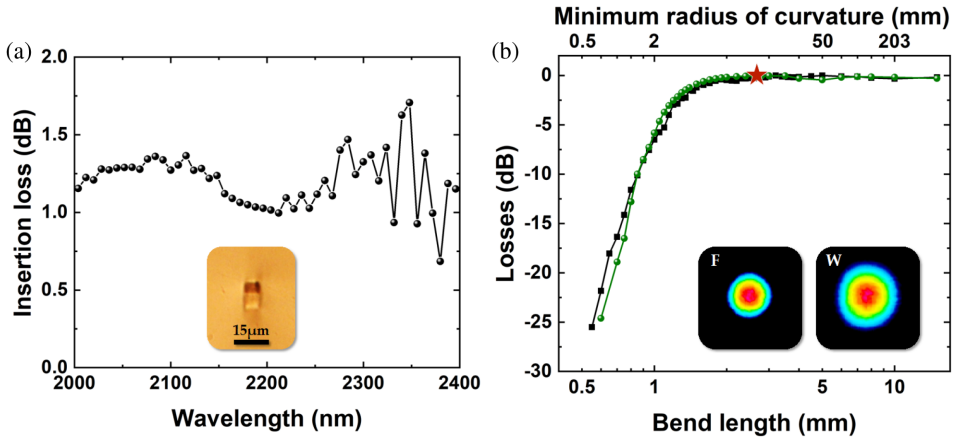

Fig. 3. (a) Insertion loss (black points) of a straight waveguide written with the best set of laser parameters where each point corresponds to a raw data average over a wavelength span of 8 nm. Inset: micrograph of the ULI waveguide. (b) Evolution of the experimental losses (black squares) in relation to the straight waveguide as a function of the bend length for a deviation of 100 μm and the simulated losses with a refractive index difference of $8 \cdot 10^{-3}$ (green points). The red star represents the radius of curvature of couplers. Inset: output near-field intensity distribution of the fiber (F) and waveguide (W).

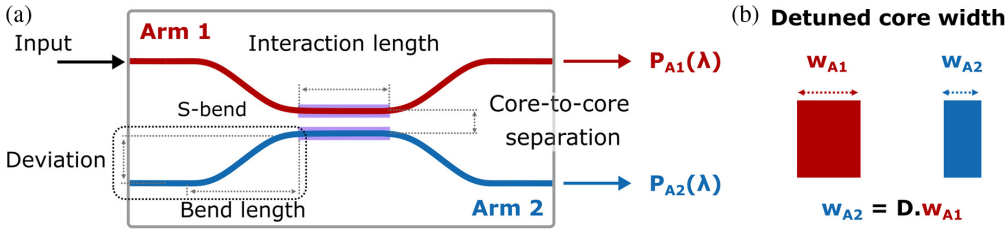

Fig. 4. (a) Schematic representation of the 3 dB asymmetric directional coupler with a description of the important geometric parameters for fabrication and characterization. (b) Illustration of waveguide width difference defined by D for the detuned core study.

measured around 8.7 μm on x axis and 8.8 μm on y axis. Using the optimal ULI parameters, we also investigated the bending-induced losses in these waveguides. To do this, we fabricated an array of 50 waveguides where each waveguide undergoes a symmetric double "S-bend" describing a "raised sinus" profile with a lateral shift deviation of 100 μm in the plane of the substrate, as presented in the dot black square labeled "S-bend" in Fig. 4(a). Figure 3(b) presents the results of experiments to characterize the bend induced losses as a function of bend length and radius of curvature. These results indicate that for a 100 μm lateral shift deviation, a bend length of 2 mm results in minimal excess loss. Calculated using CodeSeeder's BeamLab toolboxes for MATLAB and fitting the experimental bend losses [green points in Fig. 3(b)] [41], the refractive index difference of ULI waveguides is estimated at $8 \cdot 10^{-3}$.

C. Developing Asymmetric 3 dB Couplers

For all our studies, we used a substrate chip length of 17 mm, which will be sufficient in the future to fabricate the beam combiner in Fig. 1. With this in mind, we have chosen to fabricate ULI waveguides with a transverse deviation of 58.5 μm over a bend length of 2 mm providing negligible bending loss and corresponding to a minimum radius of curvature of around 14 mm [red star in Fig. 3(b)]. The multiscan fabrication process of each arm is from left to right in Fig. 3(a) where the writing laser beam is coming from the top. For the couplers, arm 1 is written first and then arm 2, from top to bottom in Fig. 4(a).

To characterize each directional coupler, the experimental setup shown in Fig. 2 was used to measure the spectrum of the light leaving each arm—$P_{A1}(\lambda)$ and $P_{A2}(\lambda)$ for arm 1 and arm 2, respectively. When coupling light into arm 1 of the coupler, the fraction of light coupled into arm 1 at each wavelength is given as $R_1(\lambda) = P_{A1}(\lambda)/(P_{A1}(\lambda) + P_{A2}(\lambda))$ and into arm 2 $R_2(\lambda) = P_{A2}(\lambda)/(P_{A1}(\lambda) + P_{A2}(\lambda))$ [42]. For all the following coupler characterization experiments, the input light is always coupled into arm 1 of the coupler, and we describe the evolution of coupling ratios $R_1(\lambda)$ and $R_2(\lambda)$. The coupling ratio of a coupler at each wavelength is dependent on two parameters: the interaction length and the core-to-core separation defined as the distance between the two core centers, in Fig. 4(a). A detailed study was performed to understand how these two parameters impact the coupling ratio by varying the interaction length from 0.05 to 1.6 mm in steps of 0.05 mm and the core-to-core separation from 9 to 15 μm in steps of 1 μm. Figure 5 presents 2D maps representing the experimental measurements of the coupling ratios $R_1(\lambda)$ (a) and $R_2(\lambda)$ (b) for couplers fabricated with a core-to-core separation of 10 μm. The color pattern gives two pieces of information: (i) a horizontal color line indicates achromatic behavior; and (ii) a white line indicates 3 dB splitting. Thus, a white horizontal line represents achromatic 3 dB behavior over the full K-band ($R(\lambda) = 0.5$). The experimental results clearly highlight the

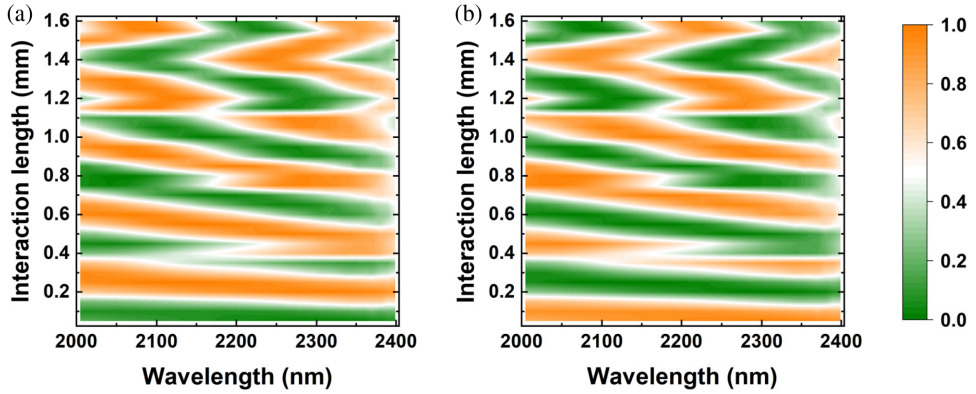

Fig. 5. 2D representation maps representing the experimental measurements providing the (a) $R_1(\lambda)$ and (b) $R_2(\lambda)$ values as a function of interaction length and propagated wavelength for a core-to-core separation of 10 μm.

impact of the interaction length on the coupling behavior in a directional coupler, with shorter interaction lengths leading to more achromatic performance. Also, one can observe the same global coupling trend with the other core-to-core separation measurements where the interaction needs to be longer to obtain the same coupling behavior for a higher core-to-core separation. Interestingly, there appears to be something of a discontinuity in the operation of the couplers once the interaction length is beyond ∼1.1 mm. This phenomenon is currently under investigation. We have performed the same experiment by coupling input light in arm 2 and a similar behavior was observed. Even though the "white line" appears to be flat and achromatic around an interaction length of 0.2 mm, a 3 dB asymmetric directional coupler is not achievable with these parameters over the full K-band.

To achieve the desired achromatic behavior, we focused our investigation on detuning the propagation constant of the guided mode in one of the waveguides in the coupler relative to the propagating mode in the other waveguide [42–45]. For the following detuned study, the investigation was carried out for all couplers with a core-to-core separation of 10 μm and the shortest interaction lengths. For our propose, the "mode-detuning" was induced by controlling the ULI process such that one of the waveguides adiabatically transitions to a smaller waveguide width as it approaches the interaction region, and then adiabatically transitions back to its original waveguide width as it leaves the coupling region. The taper length is then equal to the 2 mm bend length and is produced by adjusting the scan separation. This way, one can ensure negligeable losses along the taper transition and preserve high throughput propagation. Figure 4(b) illustrates how asymmetric directional couplers were fabricated that consisted of two waveguides—arm 1 and arm 2. Arm 1 has a width w_{A1}, and arm 2 has a width w_{A2}, which is a factor D smaller than w_{A1}. In our study, D was varied between 0.75 and 1.00 in steps of 0.05. Figures 6(a)–6(d) show the experimentally measured coupler coupling ratios (a), (c) $R_1(\lambda)$ and (b), (d) $R_2(\lambda)$ as a function of the interaction length and wavelength, with (a), (b) $D = 0.75$ and (c), (d) $D = 0.8$.

The dashed gray rectangular areas highlight the relevant interaction length that results in a close-to-3 dB achromatic behavior over the K-band for both cases. These maps show two options to obtain a 3 dB asymmetric directional coupler, one for an interaction length of 400 μm with $D = 0.75$ and one for an interaction length of 600 μm with $D = 0.8$. Over the full K-band span, Figs. 6(e) and 6(f) present the evolutions of coupling ratios $R_1(\lambda)$ (red points) and $R_2(\lambda)$ (blue diamond) of these two possible couplers for: (e) an interaction length of 400 μm with $D = 0.75$ and (f) an interaction length of 600 μm with $D = 0.8$. These results show the capability of the ULI method to provide 3 dB asymmetric directional couplers in IG for K-band applications.

4. 3 dB ASYMMETRIC ULI COUPLERS CHARACTERIZATION

As detailed previously, the 3 dB asymmetric couplers will eventually form the heart of an IO beam combining instrument to replace the existing MONA beam combiner of the JouFLU instrument at the CHARA array. To further assess their suitability for this, we used the experimental setup shown in Fig. 7 to characterize their polarization preserving and interferometric properties. A systematic characterization of all 3 dB asymmetric directional couplers written on the chip was conducted to isolate the optimal device based on the metric of the highest broadband interferometric contrast. We present the experimental results of the identified asymmetric coupler fabricated with an interaction length of 600 μm with D = 0.8.

A. Polarization Study

During the fabrication process, ultrafast laser exposure generates form and stress birefringence in the glass substrate, which may have a substantial impact on the polarization behavior of the ULI waveguides [46,47]. As differential birefringence effects between the left and right arms of the device may result in visibility losses, we investigated this aspect and developed an experimental setup to observe the polarization behavior of the coupler for a varying input linear polarization. The experimental setup is presented in the gray dotted rectangle in Fig. 7(a). K-band filtered (SBP-2314-0001112) SC light (Leukos STM 250 MIR) is passed through a wire grid polarizer (WP25M-UB) and coupled to one input of the ULI coupler. The wire grid polarizer allows us to ensure a linearly controlled polarization state at the ULI waveguide input with an extinction ratio around

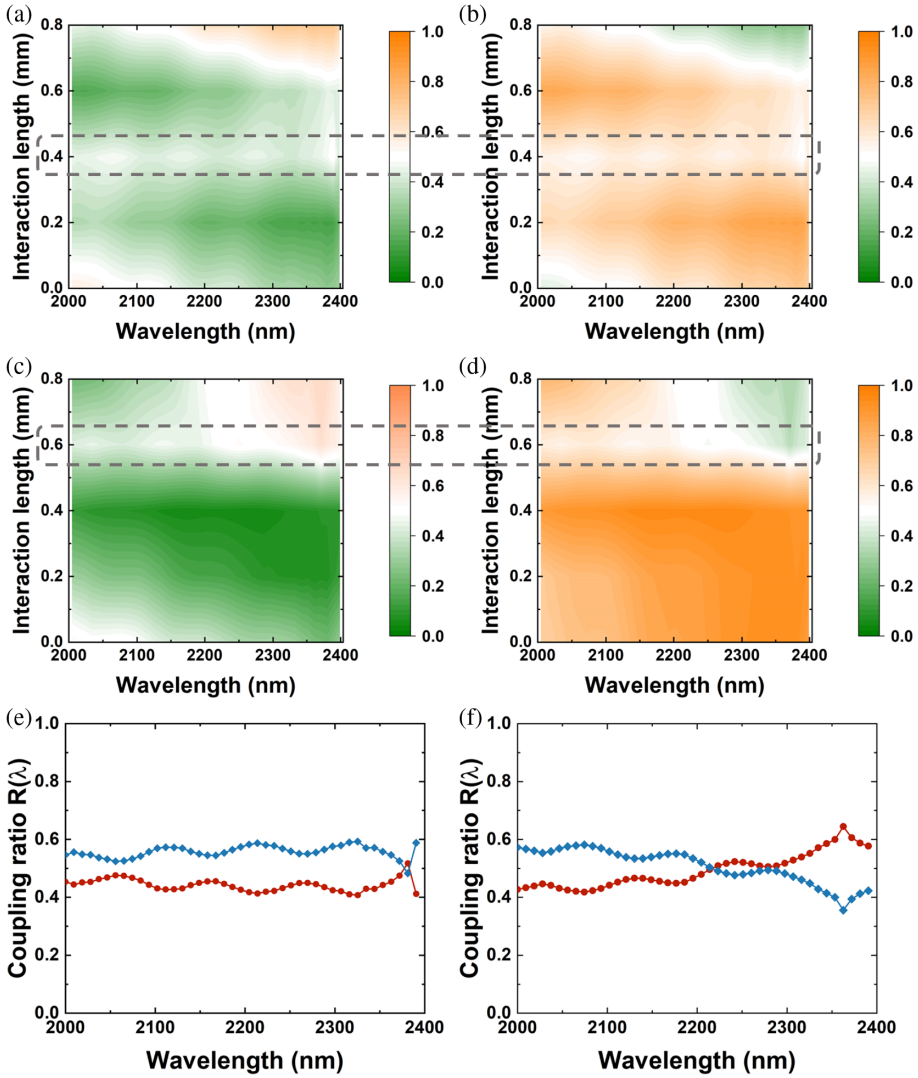

Fig. 6. 2D map representation of the full investigation of the coupling ratios (a), (c) $R_1(\lambda)$ and (b), (d) $R_2(\lambda)$ versus interaction length and propagated wavelength with (a), (b) $D = 0.75$ and (c), (d) $D = 0.8$. The dashed gray rectangle highlights the interaction length with a white horizontal power ratio line for the two arms, which represents a 3 dB asymmetric directional coupler ($R(\lambda) \sim 0.5$). Coupling ratio evolutions of $R_1(\lambda)$ in red points and $R_2(\lambda)$ in blue diamonds for (e) interaction length of 400 μm with $D = 0.75$ and (f) interaction length of 600 μm with $D = 0.8$.

30 dB over the whole K-band, even using an unpolarized SC source. The output analyzer informs us on the polarization state of the emergent light measured by the IR camera. By varying the input polarization of the coupled light with the polarizer (from 0° to 240° in steps of 20°), we investigated the polarization maintaining properties of the ULI fabricated coupler. The 0° position corresponds to the vertical direction with respect to the horizontal optics table. The polarization contrast is defined as $C_p = (I_{\mathrm{Max}} - I_{\mathrm{Min}})/(I_{\mathrm{Max}} + I_{\mathrm{Min}})$, where I_{Max} and I_{Min} are, respectively, the maximum and minimum flux measured on the IR camera (Infratech 5360S) when rotating the analyzer. Therefore, a polarization contrast $C_p = 1$ corresponds to a linear polarization, and a contrast $C_p = 0$ corresponds to a circular polarization of the output signal transmitted by the combiner. Then, intermediate values correspond to an elliptical polarization. Figures 8(a) and 8(b) present the variations in the measured polarization contrast C_p for the light collected from arm 1 and arm 2 of the asymmetric directional coupler as a function of the input linear polarization angle. With this measurement, we identify the angular positions (with respect to the horizontal plane of the optical bench) of the fast and slow axes of the birefringent coupler, which correspond to angular directions for which the linear input polarization is maintained.

We find that, within the precision of our measurement, the positions of the fast and slow axes are at about ∼80° and ∼170° for arm 1 and arm 2, respectively, and ∼ 90° apart as expected. In principle, this information can be used in the future to align the axis of the input polarization-maintaining fibers and the IO combiner. This measurement also informs us on the maximum phase retardation introduced by the coupler since $C_{p,\mathrm{min}} = \cos(\psi)$, where ψ is the phase retardation in radians. This remains true in the case of polychromatic light when we consider the relatively narrow bandwidth of the K-band filter. We find experimentally the highest retardation to be ∼80°, and as expected at about 45° from the slow/fast axis directions. Finally, we can qualitatively assess with these graphs the level of

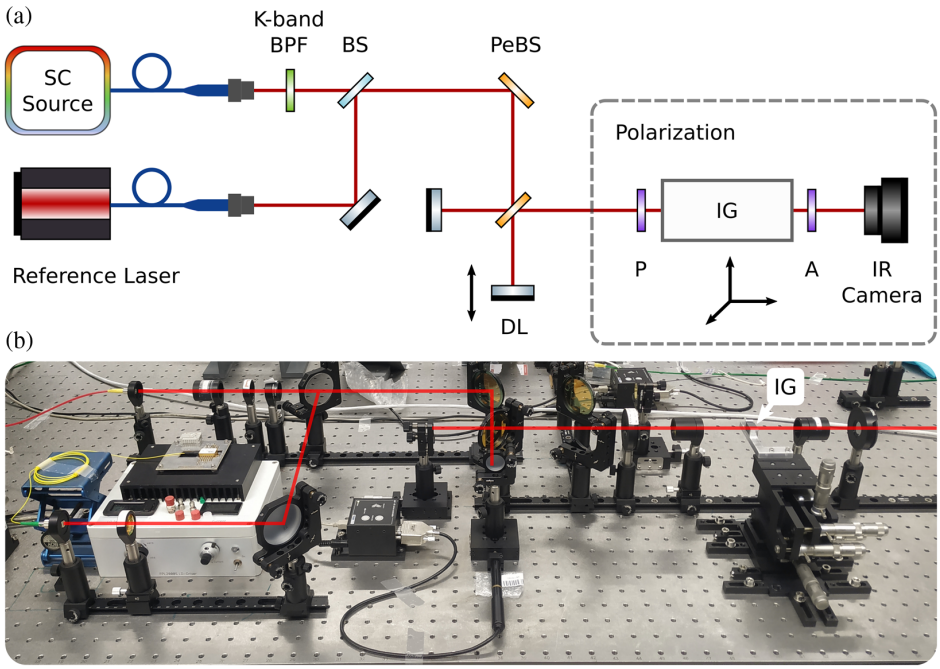

Fig. 7. (a) Schematic of the interferometry experimental setup with the two sources (SC source and reference laser at 2 μm), beam splitter (BS) to overlap the beams, followed by the interferometer based on several pellicle beam splitters (PeBS) and a delay line mirror (DL) as well as a fixed mirror. Light is then passed through a polarizer (P) before being coupled in the asymmetric directional couplers on the glass substrate, finally passing through an analyzer (A), after which an IR camera acquires the output light. (b) Photograph of the interferometry setup.

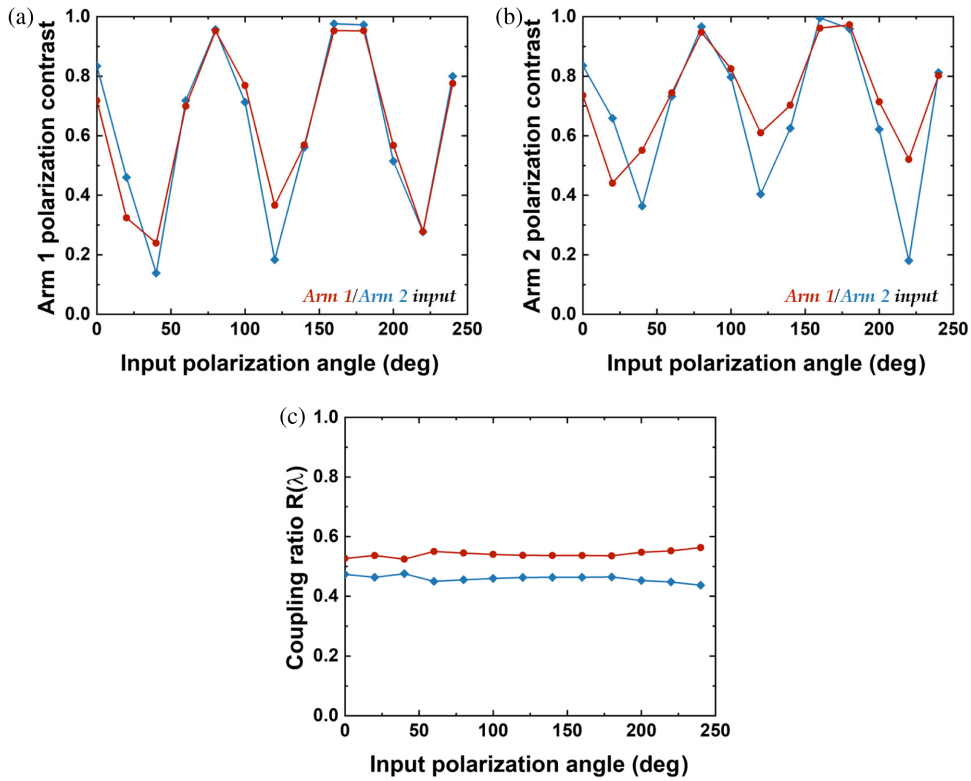

Fig. 8. (a) Evolution of the output polarization contrast in arm 1 and (b) arm 2 as a function of the input polarization angle when light is coupled to arm 1 (red point curve) or arm 2 (diamond blue curve). (c) Evolution of coupling ratios $R_1(\lambda)$ in red points and $R_2(\lambda)$ in blue diamonds as a function of the input polarization angle.

differential birefringence between the two arms of the coupler [48]. This can inform us on the possibility of visibility losses due to polarization effects. For a given output arm [Fig. 8(a) or Fig. 8(b)], the two red and blue curves should ideally be the same if no differential birefringence is present. While comparable in shape, we qualitatively observe that both outputs of the combiner are affected by some level of differential birefringence, with arm 2 (right) slightly worse than arm 1 (left). However, this level of differential birefringence will not result in a significant visibility loss as we will see in the next section, at least for classical V^2 interferometry. Finally, Fig. 8(c) shows the dependence of beam combiner coupling ratio $R(\lambda)$ with the input linear polarization direction, which is controlled by the input polarizer. No analyzer is used at the waveguide outputs in this case. We observe only a mild variation of ∼5% in the coupling ratio as a function of the input linear polarization angle, with the two curves $R(\lambda)$ showing a relatively flat profile. Again, we have performed this experiment by coupling input light in arm 2, and a similar behavior was observed. While such an effect can generally be mitigated by instrumental strategies (e.g., splitting the input horizontal and vertical polarizations), it is reassuring to observe that the intensity unbalance of the coupler is only slightly dependent on the input polarization. This may become relevant when both polarizations of the incoming beams are coupled into the chip. We believe that the polarization effects we have observed are due to stress induced birefringence in the coupler interaction region. In particular, the birefringence properties of the waveguide inscribed first, arm 1 in our case, become altered by the stress field generated by the inscription of the second waveguide arm 2 [49,50]. The impact of this stress field is observed in the discrepancy of polarization contrast at the output of the two arms, as presented in Figs. 8(a) and 8(b).

B. Interferometry Measurements

The interferometric bench setup (Fig. 7) is based on a SC source followed by a K-band BPF and a reference continuous wave laser diode emitting at 2 μm, which can be aligned with the broadband source by tilting a beam splitter (BS). The bench is based on a classical two-channel interferometric setup, described in more detail in [51]. A polarizer can be placed in the input beam to change the linear polarization angle before coupling light in the coupler. The delay line scans the fringes over 100 μm [±50 μm around the zero optical path difference (OPD)] at a speed of 0.5 μm per second, and the data are recorded at 250 Hz. Figure 9(a) presents the interferogram patterns recorded for the two arms of the 3 dB asymmetric directional coupler. The total length of the fringe packet is about 200 μm, double the scan range, because of mirror reflection. Figure 9(b) shows a close-up view of the central OPD region, where the π-phase shift between the two outputs of the coupler is clearly visible. The interferogram shows some noise contribution at the position of successive maxima. Before deriving the instrumental contrast, we reduced the impact of the high-frequency noise by applying the Savitzky–Golay (SG) smoothing and differentiation filtering method [52]. Following this step, the broadband instrumental contrast was measured to be 92%, which is represented by the dark curves and the dashed gray lines in Fig. 9(b). Following the analysis presented Section 4.A, we investigated the dependence of the interferometric contrast with the angular direction of the input linear polarization.

For this purpose, three measurements were acquired with input linear polarization angles of 0°, 45°, and 90°, and we find that in all three cases, the contrast is ≥92%. In absence of a measurement of the bare contrast of the test bench, the contrast of 92% should be understood as a current upper limit of the performance of the beam combiner. Further and more detailed characterization of the intrinsic performance of the bench [51] could help to disentangle more precisely the contributions to be attributed to the beam combiner and refine the ultimate achievable performances of the device. Our analysis shows that the ULI platform can deliver high-quality K-band IO beam combiners with high instrumental contrast, which are relatively polarization insensitive.

5. CONCLUSION

We reported the development of 3 dB asymmetric directional couplers that operate across the full K-band between 2.0 and 2.4 μm for future stellar interferometry applications. The couplers were fabricated in a commercial IG using ULI with optimized parameters, with straight waveguides exhibiting an insertion loss of ∼1.2 ± 0.5 dB over the K-band with single-mode behavior. A number of asymmetric directional couplers

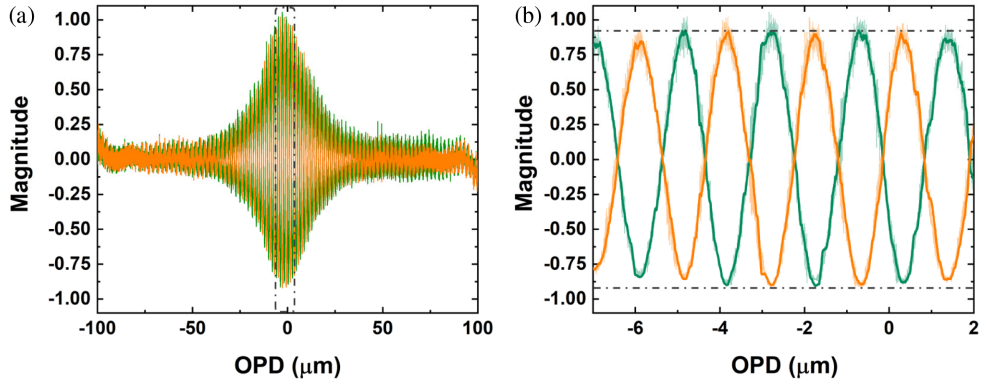

Fig. 9. (a) Full interferometer pattern recorded for the two arms of the 3 dB asymmetric directional coupler and a close-up in the dashed rectangular region (b) using a FFT filtering correction. (b) Close-up of (a) showing the noisy FFT correction in the background as transparent curves and the SG results as dark curves, corresponding to a contrast magnitude of 92%.

with different interaction lengths and geometric properties were studied to achieve the best device, which exhibits 3 dB achromatic splitting behavior over the K-band. We presented the results of characterization experiments, which demonstrate that the birefringence axes of the coupler waveguides are not aligned with each other and are not aligned with the substrate axis. Finally, two successive filtering corrections (FFT and SG) provide a high contrast magnitude of 92%. The results demonstrate that ULI can fabricate high-quality asymmetric directional couplers for applications in K-band astronomical interferometry. We aim to use these devices to develop a complete two-telescope K-band IO beam combiner system to replace the existing beam combiner MONA in JouFLU at the CHARA array. The ULI fabrication method can be easily adapted to fabricate a 3D multi-telescope interferometer in K-band.

Funding. Horizon 2020 Framework Programme (730890-OPTICON); H2020 Future and Emerging Technologies (820365-PHoG); Bundesministerium für Bildung und Forschung (03Z22AN11); Deutsche Forschungsgemeinschaft (326946494); National Science Foundation (AST-1636624, AST-1715788); Science and Technology Facilities Council (ST/N000625/1); Engineering and Physical Sciences Research Council (iCase studentship part funded by Renishaw).

Acknowledgment. FAP acknowledges support via an EPSRC iCASE studentship funded by Renishaw. RRT sincerely thanks LightConversion for its support. Institutional support has been provided from the GSU College of Arts and Sciences and the GSU Office of the Vice President for Research and Economic Development.

Disclosures. The authors declare no conflicts of interest.

Data Availability. Data underlying the results presented in this paper are not publicly available at this time but may be obtained from the authors upon reasonable request.

[†]These authors contributed equally to this paper.

REFERENCES

1. J. Bland-Hawthorn and P. Kern, "Astrophotonics: a new area for astronomical instruments," Opt. Express **17**, 1880–1884 (2009).
2. V. Coudé du-Foresto and S. T. Ridgway, "FLUOR–a Stellar interferometer using single-mode fibers," in *European Southern Observatory Astrophysics Symposia*, J. M. Beckers and F. Merkle, eds. (1992), Vol. **39**, p. 731.
3. V. Coudé du Foresto, G. Perrin, J.-M. Mariotti, M. Lacasse, and W. Traub, "The FLUOR/IOTA fiber stellar interferometer," in *Integrated Optics for Astronomical Interferometry*, P. Kern and F. Malbet, eds. (1997), pp. 115–125.
4. K. Rousselet-Perraut, P. Haguenauer, P. Petmezakis, J.-P. Berger, D. Mourard, S. D. Ragland, G. Huss, F. Reynaud, E. LeCoarer, P. Y. Kern, and F. Malbet, "Qualification of IONIC (integrated optics nearinfrared interferometric camera)," Proc. SPIE **4006**, 1042–1051 (2000).
5. I. J. Lewis, R. D. Cannon, K. Taylor, K. Glazebrook, J. A. Bailey, I. K. Baldry, J. R. Barton, T. J. Bridges, G. B. Dalton, T. J. Farrell, P. M. Gray, A. Lankshear, C. McCowage, I. R. Parry, R. M. Sharples, K. Shortridge, G. A. Smith, J. Stevenson, J. O. Straede, L. G. Waller, J. D. Whittard, J. K. Wilcox, and K. C. Willis, "The Anglo-Australian observatory 2dF facility," Mon. Not. R. Astron. Soc. **333**, 279–298 (2002).
6. M. M. Roth, A. Kelz, T. Fechner, T. Hahn, S.-M. Bauer, T. Becker, P. Böhm, L. Christensen, F. Dionies, J. Paschke, E. Popow, D. Wolter, J. Schmoll, U. Laux, and W. Altmann, "PMAS: The Potsdam multi-aperture spectrophotometer. I. Design, manufacture, and performance," Publ. Astron. Soc. Pac. **117**, 620 (2005).
7. A. Kelz, M. A. W. Verheijen, M. M. Roth, S. M. Bauer, T. Becker, J. Paschke, E. Popow, S. F. Sánchez, and U. Laux, "PMAS: the Potsdam multi-aperture spectrophotometer. II. The wide integral field unit PPak," Publ. Astron. Soc. Pac. **118**, 129 (2006).
8. M. T. Murphy, T. Udem, R. Holzwarth, A. Sizmann, L. Pasquini, C. Araujo-Hauck, H. Dekker, S. D'Odorico, M. Fischer, T. W. Hänsch, and A. Manescau, "High-precision wavelength calibration of astronomical spectrographs with laser frequency combs," Mon. Not. R. Astron. Soc. **380**, 839–847 (2007).
9. A. Stoll, Y. Wang, and K. Madhav, "Integrated Echelle gratings for astrophotonics," Proc. SPIE **11203**, 112030Z (2020).
10. M. Mayor, F. Pepe, D. Queloz, F. Bouchy, G. Rupprecht, G. Curto, G. A. Avila, W. Benz, J. Bertaux, X. Bonfils, T. Dall, H. Dekker, B. Delabre, W. Eckert, M. Fleury, A. Gilliotte, D. Gojak, J. Guzman, D. Kohler, J. Lizon, A. Longinotti, C. Lovis, D. Mégevand, L. Pasquini, and J. Reyes, "Setting new standards with HARPS," Messenger **114**, 20–24 (2003).
11. N. Cvetojevic, N. Jovanovic, J. Lawrence, M. Withford, and J. Bland-Hawthorn, "Developing arrayed waveguide grating spectrographs for multi-object astronomical spectroscopy," Opt. Express **20**, 2062–2072 (2012).
12. C. Q. Trinh, S. C. Ellis, J. Bland-Hawthorn, J. S. Lawrence, A. J. Horton, S. G. Leon-Saval, K. Shortridge, J. Bryant, S. Case, M. Colless, W. Couch, K. Freeman, H.-G. Loehmannsroeben, L. Gers, K. Glazebrook, R. Haynes, S. Lee, J. O'Byrne, and S. Miziar, "GNOSIS: The first instrument to use fiber Bragg gratings for OH suppression," Astron. J. **145**, 51 (2013).
13. N. Jovanovic, N. Cvetojevic, B. Norris, C. Betters, C. Schwab, J. Lozi, O. Guyon, S. Gross, F. Martinache, P. Tuthill, D. Doughty, Y. Minowa, N. Takato, and J. Lawrence, "Demonstration of an efficient, photonic-based astronomical spectrograph on an 8-m telescope," Opt. Express **25**, 17753–17766 (2017).
14. J. Bland-Hawthorn, M. Englund, and G. Edvell, "New approach to atmospheric OH suppression using an aperiodic fibre Bragg grating," Opt. Express **12**, 5902–5909 (2004).
15. M.-G. Suh, X. Yi, Y. H. Lai, S. Leifer, I. S. Grudinin, G. Vasisht, E. C. Martin, M. P. Fitzgerald, G. Doppmann, J. Wang, D. Mawet, S. B. Papp, S. A. Diddams, C. Beichman, and K. Vahala, "Searching for exoplanets using a microresonator astrocomb," Nat. Photonics **13**, 25–30 (2019).
16. H. A. McAlister, W. G. Bagnuolo, Jr., W. I. Hartkopf, and A. K. Garrison, "Multiple-telescope optical interferometric array," Proc. SPIE **1237**, 22–30 (1990).
17. F. Eisenhauer, G. Perrin, W. Brandner, C. Straubmeier, K. Perraut, A. Amorim, M. Schöller, S. Gillessen, P. Kervella, M. Benisty, C. Araujo-Hauck, L. Jocou, J. Lima, G. Jakob, M. Haug, Y. Clénet, T. Henning, A. Eckart, J. Berger, P. Garcia, R. Abuter, S. Kellner, T. Paumard, S. Hippler, S. Fischer, T. Moulin, J. Villate, G. Ávila, A. Gräter, S. Lacour, A. Huber, M. Wiest, A. Nolot, P. Carvas, R. Dorn, O. Pfuhl, E. Gendron, S. Kendrew, S. Yazici, S. Antón, Y. Jung, M. Thiel, E. Choquet, R. Klein, P. Teixeira, P. Gitton, D. Moch, F. Vincent, N. Kudryavtseva, S. Ströbele, E. Sturm, P. Fédou, R. Lenzen, P. Jolley, C. Kister, V. Lapeyrère, V. Naranjo, C. Lucuix, R. Hofmann, F. Chapron, U. Neumann, L. Mehrgan, O. Hans, G. Rousset, J. Ramos, M. Suárez, R. Lederer, J. Reess, R. Rohloff, P. Haguenauer, H. Bartko, A. Sevin, K. Wagner, J. Lizon, S. Rabien, C. Collin, G. Finger, R. Davies, D. Rouan, M. Wittkowski, K. Dodds-Eden, D. Ziegler, F. Cassaing, H. Bonnet, M. Casali, R. Genzel, and P. Léna, "GRAVITY: observing the universe in motion," Messenger **143**, 16 (2011).
18. M. Benisty, J.-P. Berger, L. Jocou, P. Labeye, F. Malbet, K. Perraut, and P. Kern, "An integrated optics beam combiner for the second generation VLTI instruments," Astron. Astrophys. **498**, 601–613 (2009).
19. M. Schöller, "The Very Large Telescope Interferometer: current facility and prospects," New Astron. Rev. **51**, 628–638 (2007).
20. J. D. Monnier, A. Aarnio, O. Absil, N. Anugu, E. Baines, A. Bayo, J.-P. Berger, L. I. Cleeves, D. Dale, W. Danchi, W. J. de Wit, D. Defrère, S. Domagal-Goldman, M. Elvis, D. Froebrich, M. Gai, P. Gandhi, P. Garcia, T. Gardner, D. Gies, J.-F. Gonzalez, B. Gunter, S. Hoenig, M. Ireland, A. M. Jorgensen, M. Kishimoto, L. Klarmann, B. Kloppenborg, J. Kluska, J. S. Knight, Q. Kral, S. Kraus, L. Labadie, P. Lawson, J.-B. Le Bouquin, D. Leisawitz, E. G. Lightsey, H. Linz, S. Lipscy, M. MacGregor, H. Matsuo, B. Mennesson, M. Meyer, E. A. Michael, F. Millour, D. Mozurkewich, R. Norris, M. Ollivier, C.

Packham, R. Petrov, L. Pueyo, B. Pope, S. Quanz, S. Ragland, G. Rau, Z. Regaly, A. Riva, R. Roettenbacher, G. Savini, B. Setterholm, M. Sewilo, M. Smith, L. Spencer, T. ten Brummelaar, N. Turner, G. van Belle, G. Weigelt, and M. Wittkowski, "A realistic roadmap to formation flying space interferometry," Astro2020 APC White Paper, arXiv: 1907.09583 (2019).
21. S. Piacentini, T. Vogl, G. Corrielli, P. K. Lam, and R. Osellame, "Space qualification of ultrafast laser-written integrated waveguide optics," Laser Photon. Rev. **15**, 2000167 (2020).
22. K. Perraut, L. Jocou, J. P. Berger, A. Chabli, V. Cardin, G. Chamiot-Maitral, A. Delboulbé, F. Eisenhauer, Y. Gambérini, S. Gillessen, S. Guieu, J. Guerrero, M. Haug, F. Hausmann, F. Joulain, P. Kervella, P. Labeye, S. Lacour, C. Lanthermann, V. Lapras, J. B. Le Bouquin, M. Lippa, Y. Magnard, T. Moulin, P. Noël, A. Nolot, F. Patru, G. Perrin, O. Pfuhl, S. Pocas, S. Poulain, C. Scibetta, E. Stadler, R. Templier, N. Ventura, C. Vizioz, A. Amorim, W. Brandner, and C. Straubmeier, "Single-mode waveguides for GRAVITY–I. The cryogenic 4-telescope integrated optics beam combiner," Astron. Astrophys. **614**, A70 (2018).
23. GRAVITY Collaboration, "First light for GRAVITY: phase referencing optical interferometry for the Very Large Telescope Interferometer," Astron. Astrophys. **602**, A94 (2017).
24. L. Jocou, K. Perraut, A. Nolot, T. Moulin, Y. Magnard, P. Labeye, V. Lapras, F. Eisenhauer, G. Perrin, A. Amorim, W. Brandner, and C. Straubmeier, "The integrated optics beam combiner assembly of the GRAVITY/VLTI instrument," Proc. SPIE **8445**, 84452X (2012).
25. O. Humbach, H. Fabian, and U. Grzesik, "Analysis of OH absorption bands in synthetic silica," J. Non-Crys. Sol. **203**, 19–26 (1996).
26. L. Labadie and O. Wallner, "Mid-infrared guided optics: a perspective for astronomical instruments," Opt. Express **17**, 1947–1962 (2009).
27. W. A. Traub and K. W. Jucks, "A possible aeronomy of extrasolar terrestrial planets," arXiv: 0205369 (2002).
28. N. Jovanovic, P. G. Tuthill, and B. Norris, "Starlight demonstration of the Dragonfly instrument: an integrated photonic pupil-remapping interferometer for high-contrast imaging," Mon. Not. R. Astron. Soc. **427**, 806–815 (2012).
29. J. Tepper, L. Labadie, S. Gross, A. Arriola, S. Minardi, R. Diener, and M. J. Withford, "Ultrafast laser inscription in ZBLAN integrated optics chips for mid-IR beam combination in astronomical interferometry," Opt. Express **25**, 20642–20653 (2017).
30. F. A. Pike, A. Benoît, D. G. MacLachlan, R. J. Harris, I. Gris-Sánchez, D. Lee, T. A. Birks, and R. R. Thomson, "Modal noise mitigation for high-precision spectroscopy using a photonic reformatter," Mon. Not. R. Astron. Soc. **497**, 3713–3725 (2020).
31. S. Haffert, R. J. Harris, A. Zanutta, F. A. Pike, A. Bianco, E. M. A. Redaelli, A. Benoît, D. G. MacLachlan, C. A. Ross, I. Gris-Sánchez, M. D. Trappen, Y. Xu, M. Blaicher, P. Maier, G. Riva, B. Sinquin, C. Kulcsár, N. A. Bharmal, É. Gendron, L. Staykov, T. J. Morris, S. Barboza, N. Münch, L. F. Bardou, L. Prengère, H.-F. G. Raynaud, P. Hottinger, T. Anagnos, J. Osborn, C. Koos, R. R. Thomson, T. A. Birks, I. A. G. Snellen, and C. U. Keller, "Diffraction-limited integral-field spectroscopy for extreme adaptive optics systems with the multicore fiber-fed integral-field unit," J. Astron. Telesc. Instrum. Syst. **6**, 045007 (2020).
32. B. R. M. Norris, N. Cvetojevic, T. Lagadec, N. Jovanovic, S. Gross, A. Arriola, T. Gretzinger, M.-A. Martinod, O. Guyon, J. Lozi, M. J. Withford, J. S. Lawrence, and P. Tuthill, "First on-sky demonstration of an integrated-photonic nulling interferometer: the GLINT instrument," Mon. Not. R. Astron. Soc. **491**, 4180–4193 (2020).
33. T. A. ten Brummelaar, H. A. McAlister, S. T. Ridgway, W. G. Bagnuolo, Jr., N. H. Turner, L. Sturmann, J. Sturmann, D. H. Berger, C. E. Ogden, R. Cadman, W. I. Hartkopf, C. H. Hopper, and M. A. Shure, "First results from the CHARA array. II. Description of the instrument," Astron. J. **628**, 453–465 (2005).
34. N. J. Scott, R. Millan-Gabet, E. Lhomé, T. A. Ten Brummelaar, V. Coudé Du Foresto, J. Sturmann, and L. Sturmann, "Jouvence of FLUOR: upgrades of a fiber bean combiner at the CHARA array," J. Astron. Instrum. **2**, 1340005 (2013).
35. P. D. Nuñez, N. J. Scott, B. Mennesson, O. Absil, J.-C. Augereau, G. Bryden, T. ten Brummelaar, S. Ertel, V. Coudé du Foresto, S. T. Ridgway, J. Sturmann, L. Sturmann, N. J. Turner, and N. H. Turner, "A near-infrared interferometric survey of debris-disc stars," Astron. Astrophys. **608**, A113 (2017).
36. P. D. Nuñez, T. ten Brummelaar, B. Mennesson, and N. J. Scott, "Visibility estimation for the CHARA/JouFLU Exozodi survey," Publ. Astron. Soc. Pac. **129**, 024002 (2017).
37. J. B. LeBouquin, K. Rousselet-Perraut, P. Kern, F. Malbet, P. Haguenauer, P. Kervella, I. Schanen, J. P. Berger, A. Delboulbé, B. Arezki, and M. Schöller, "First observations with an H-band integrated optics beam combiner at the VLTI," Astron. Astrophys. **424**, 719–726 (2004).
38. M. Olivero, M. Svalgaard, L. Jocou, and J.-P. Berger, "Direct UV-written integrated optical beam combiner for stellar interferometry," J. Lightwave Technol. **25**, 367–371 (2007).
39. G. Brown, R. R. Thomson, A. K. Kar, N. D. Psaila, and H. T. Bookey, "Ultrafast laser inscription of Bragg-grating waveguides using the multiscan technique," Opt. Lett. **37**, 491–493 (2012).
40. A. Arriola, S. Mukherjee, D. Choudhury, L. Labadie, and R. R. Thomson, "Ultrafast laser inscription of mid-IR directional couplers for stellar interferometry," Opt. Lett. **39**, 4820–4822 (2014).
41. https://www.codeseeder.com/.
42. W. J. Chen, S. M. Eaton, H. Zhang, and P. R. Herman, "Broadband directional couplers fabricated in bulk glass with high repetition rate femtosecond laser pulses," Opt. Express **16**, 11470–11480 (2008).
43. A. Takagi, K. Jinguji, and M. Kawachi, "Design and fabrication of broad-band silica-based optical waveguide couplers with asymmetric structure," IEEE J. Quantum Electron. **28**, 848–855 (1992).
44. T. Gretzinger, S. Gross, A. Arriola, T. T. Fernandez, D. Strixner, J. Tepper, L. Labadie, and M. J. Withford, "Broadband mid-infrared directional and multimode interference couplers in GLS glass fabricated using femtosecond laser direct-writing," in *Conference on Lasers and Electro-Optics (CLEO)* (2019), paper cm_4_1.
45. M. Olivero and M. Svalgaard, "Direct UV-written broadband directional planar waveguide couplers," Opt. Express **13**, 8390–8399 (2005).
46. L. A. Fernandes, J. R. Grenier, P. R. Herman, J. S. Aitchison, and P. V. S. Marques, "Femtosecond laser writing of waveguide retarders in fused silica for polarization control in optical circuits," Opt. Express **19**, 18294–18301 (2011).
47. L. A. Fernandes, J. R. Grenier, P. R. Herman, J. S. Aitchison, and P. V. S. Marques, "Stress induced birefringence tuning in femtosecond laser fabricated waveguides in fused silica," Opt. Express **20**, 24103–24114 (2012).
48. R. Diener, S. Nolte, T. Pertsch, and S. Minardi, "Effects of stress on neighboring laser written waveguides in gallium lanthanum sulfide," Appl. Phys. Lett. **112**, 111908 (2018).
49. J. Tepper, L. Labadie, R. Diener, S. Minardi, J.-U. Pott, R. Thomson, and S. Nolte, "Integrated optics prototype beam combiner for long baseline interferometry in the L and M bands," Astron. Astrophys. **602**, A66 (2017).
50. G. Corrielli, S. Atzeni, S. Piacentini, I. Pitsios, A. Crespi, and R. Osellame, "Symmetric polarization-insensitive directional couplers fabricated by femtosecond laser writing," Opt. Express **26**, 15101–15109 (2018).
51. J. Tepper, R. Diener, L. Labadie, S. Minardi, S. Gross, A. Arriola, M. Withford, and S. Nolte, "Photonics-based mid-infrared interferometry: the challenges of polychromatic operation and comparative performances," Proc. SPIE **10701**, 107011B (2018).
52. A. Savitzky and M. J. E. Golay, "Soothing and differentiation of data by simplified least squares procedures," Anal. Chem. **36**, 1627–1639 (1964).